Three-dimensional double deck meshlike dye-sensitized solar cells

Yuanhao Wang, Hongxing Yang, and Lin Lu

Related Articles

A transmission line model for the optical simulation of multilayer structures and its application for oblique illumination of an organic solar cell with anisotropic extinction coefficient
J. Appl. Phys. 110, 114506 (2011)

Polymer solar cells with gold nanoclusters decorated multi-layer graphene as transparent electrode
APL: Org. Electron. Photonics 4, 259 (2011)

Polymer solar cells with gold nanoclusters decorated multi-layer graphene as transparent electrode
Appl. Phys. Lett. 99, 223302 (2011)

Cliff-like conduction band offset and KCN-induced recombination barrier enhancement at the CdS/Cu2ZnSnS4 thin-film solar cell heterojunction
Appl. Phys. Lett. 99, 222105 (2011)

Effect of a symmetry breaking layer on the open circuit voltage of conventional bulk-heterojunction solar cells
Appl. Phys. Lett. 99, 213302 (2011)

Additional information on J. Appl. Phys.

Three-dimensional double deck meshlike dye-sensitized solar cells

Yuanhao Wang, Hongxing Yang,[a] and Lin Lu
*Department of Building Service Engineering, Renewable Energy Research Group (RERG),
The Hong Kong Polytechnic University, Hong Kong, China*

In this paper, we develop a new type of three-dimensional dye-sensitized solar cells (3D DSSCs) with double deck cylindrical Ti meshes as the substrates. One of the Ti meshes is anodized to *in situ* synthesize the self-organized TiO_2 nanotube layer as the photoanode materials. Another Ti mesh is platinized through electrodeposition as the counter electrode. The morphologies of the electrodes are characterized by scanning electron microscopy. We investigate the effect of the mesh number on the 3D DSSCs with the dye adsorption, cyclic voltammetry, and electrochemical impedance spectroscopy. The results show that with the increase in the mesh number, the dye-loadings on the photoanode and the active surface area of Pt on the counter electrode are increased, while the diffusion of the electrolyte becomes more difficult due to the reduced diameter of the openings in the mesh. It has also been demonstrated that the performance of this 3D DSSC is independent of the incident solar beam angle due to its axial symmetrical structure. In the I-V measurement, the 3D DSSC based on the 90-mesh photoanode and the 120-mesh counter electrode shows the highest conversion efficiency of 5.5% under standard AM 1.5 sunlight. The problems of electrical insulator layer are discussed and further investigation is expected. © *2010 American Institute of Physics*. [doi:10.1063/1.3486222]

I. INTRODUCTION

At the beginning of this century, with the rapid economic growth in the emerging markets such as China and India, energy problem has been seen much more challenge than before due to large consumption of fossil fuel energy resources. In this case, it is essential to develop renewable energy technology such as solar cells which convert sunlight into electric energy directly. However, traditional silicon p-n junction solar cells usually require high purity silicon and ultraclean chamber, which dramatically increases the production costs.[1] The dye-sensitized solar cells (DSSCs), since reported by Gratzel in 1991,[2] have been taken as one of the most promising power sources for a new generation of solar cells due to their relatively low manufacturing cost and high energy conversion efficiency with a facile fabrication process.[3] For example, they do not need "free of dust" conditions compared with silicon-based solar cells.

Typically, the basic DSSC is built up as flat-type sandwichlike structure which consists of a transparent conductive oxide (TCO) glass such as F-doped SnO_2 glass covered with mesoporous nanocrystalline TiO_2, dye molecules attached to the surface of TiO_2, an electrolyte containing a redox couple (I^-/I_3^-), and a counter electrode such as a platinized TCO glass. Although the reported highest energy conversion efficiencies over 10% have been achieved on this type of DSSCs,[4,5] the actual area of the cell is very tiny (no more than 0.5 cm^2) because of the resistance limitation of the TCO glass.[6] Consequently, how to increase the cell area with no efficiency reduction becomes a prospective research topic. Moreover, some investigations have also reported that the cost of the TCO glass suitable for DSSCs is estimated to be 16%–24% of the total cost of the solar cell,[7] which means that the TCO glass is one of the expensive components of the DSSCs. One promising solution is to replace the TCO glass of the counter electrode side with a metal substrate[8] on account of its low resistance, low cost and high temperature sinterability, especially with the view of large-scale industrialization of the DSSCs. Fang *et al.*[9] used stainless steel as the counter electrode substrate to make the fill factor (FF) and conversion efficiency for large scale DSSCs improved by 20% because of the reduced internal resistance. Another approach is to replace the TCO substrate of photoanode with metal sheet and sunlight irradiates to the DSSC through its counter electrode side (the Pt-sputtered TCO substrate) which is at the opposite side to traditional DSSCs and this type of cells is also named as backside illuminated DSSCs.[10] However, the sunlight intensity absorbed by the dye-sensitized TiO_2 layer in the backside illuminated DSSC is poor owing to the low transmittance of the Pt-sputtered TCO glass and the high absorbance of the electrolyte. Besides, the resistance limitation problem of the TCO/metal substrates based DSSCs has not been completely resolved since there is still a TCO glass as the substrate of the electrode and the sheet resistance is only half reduced. It is surely attractive but of great challenge to realize the DSSC based on all metal substrates. Zou *et al.*[11] reported the conductive mesh based flexible DSSCs, which was the first generation of the all-metal-substrate DSSCs. They fabricated the all-metal-substrate DSSC by using stainless steel meshes as substrates and coated them with TiO_2 (photoanode) and platinum (counter electrode), respectively. By using this new structure, sunlight can easily pass through the anode and is dispersed uniformly inside the electrode. However, the conversion efficiency was only about 1.49% (100 $mW\ cm^{-2}$). On the other side, nowadays most solar cells, especially the DSSCs,

---

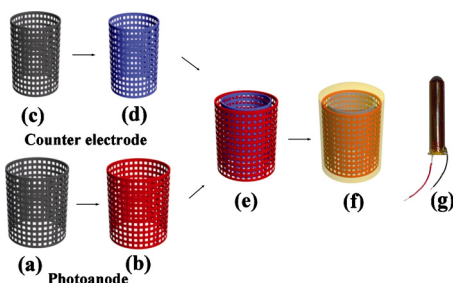[a]Electronic mail: behxyang@polyu.edu.hk.

FIG. 1. (Color online) Schematic flow diagram for the fabrication of the 3D DSSC: (a) The Ti mesh cylinder as the substrate of photoanode. (b) The sensitized photoanode. (c) The Ti mesh cylinder as the substrate of counter electrode. (d) The counter electrode based on platinized Ti mesh cylinder. (e) Double deck meshlike electrodes. (f) A sealed 3D DSSC. (g) A fabricated 3D DSSC with lead wires.

are based on two-dimensional configuration which not only restricts the absorbance of sunlight but also causes the large occupation of land. Facing these issues, it is significant to develop solar cells based on three-dimensional (3D) configuration. Taking these two points together, our previous work[11–13] has reported a 3D double helix structured all-Ti DSSC aiming toward best utilization of sunlight, reduction in the sheet resistance and the fabrication cost. This type of DSSCs whose electrodes are based on spiral Ti wires has shown its unique photovoltaic characteristics due to its special components and structures.

In this study, we will demonstrate the fabrication of an innovative all-Ti 3D DSSC by utilizing the cylindrical Ti meshes as the substrates of electrodes combined with the electrochemical anodization method to *in situ* synthesize self-organized TiO_2 nanotubes as the photoanode material. The vertically self-organized TiO_2 nanotubes with controllable lengths could provide high specific surface area to load more dye molecules and unidirectional grain boundary free pathways for the photogenerated electrons transportation,[14] which would increase the charge collection efficiency. Moreover, the holes in the meshes could not only increase the exposure area of the substrates but also provide transportation channels for the electrolyte. In addition, the 3D cylindrical structure of the DSSC is able to capture more sunlight compared with the flat-type devices.

II. EXPERIMENTAL

Three types of Ti meshes (60-mesh, 90-mesh, and 120-mesh) were used as the substrates of the photoanodes. The 60-mesh means that there are 60 openings in 1 in^2 of mesh. With the increase in the mesh number, the diameter of the openings will be decreased. The meshes were first cut into square pieces, and then folded along a metal nail to form the Ti mesh cylinders. The two edges were connected by employing a Ti wire to wound them together and the diameter of the cylinder is about 4 mm, which can be seen from Fig. 1(a). Before anodization, the Ti mesh cylinder was cleaned in ultrasonic baths with ethanol first and then de-ionized water for 3 min each to remove surface contaminants. The anodization was performed in a two-electrode configuration with the Ti mesh cylinder as the working electrode to grow the TiO_2 nanotube films and platinum foil as the counter elec-

trode under constant potential (30 V) at room temperature (23 °C). A direct current power supply (Agilent E3612A) was to drive the anodization process. The electrode was anodized in the electrolyte containing a mixture of ethylene glycol (50.86 wt %), polyethylene glycol 600 (47.38 wt %), H_2O (1.31 wt %), and NH_4F (0.43 wt %). In order to achieve different thicknesses of the TiO_2 nanotube films, anodization time was arranged from 10 to 80 h. After anodization, the anodized samples were rinsed with de-ionized water and treated in oxygen ambient at 480 °C for 3 h, with heating and cooling rates of 2 °C min^{-1}. After that the samples were immersed in a 0.05M $TiCl_4$ aqueous solution at 70 °C for 30 min, and subsequently rinsed in ethanol and annealed in air at 450 °C for 30 min. Finally, the anodized Ti mesh cylinders were immersed in a mixture solution of tert-butyl alcohol and acetonitrile (1:1 in volume) of $5 \times 10^{-4}M$ cis-bis (isothiocyanato) bis(2,2′-bipyrridyl-4-4′-dicarboxylato)-ruthenium(II) bis-tetrabutylammonium dye (N-719, Solaronix) to get sensitized, as shown in Fig. 1(b). After 24 h, the sensitized samples were rinsed with ethanol to remove nonchemisorbed dyes.

The preparation method of the counter electrodes was almost the same as the photoanodes. In short, three types of Ti meshes (60-mesh, 90-mesh, and 120-mesh) were folded into Ti mesh cylinders, while the only difference is the smaller diameter of the cylinder, 2.5 mm, as shown in Fig. 1(c). They were then washed with acetone and ethanol in an ultrasonic bath for 3 min. The Pt thin film was deposited onto the titanium surface by an electrodeposition process which was carried out using an aqueous solution of $5 \times 10^{-3}M$ $H_2PtCl_6 \cdot 6H_2O$ at room temperature. A digital sourcemeter (Keithley, 2400) was applied as a power supply. Here, the Pt counter electrode [Fig. 1(d)] was prepared with 15 mA cm^{-2} current density for 30 s.

For the solar cell fabrication, the counter electrode (platinized Ti mesh cylinder) was first sprayed with a porous SiO_2 layer as an electrical insulator,[15] and then inserted into the internal hole of the photoanode (anodized Ti mesh cylinder sensitized with dye molecules), as shown in Fig. 1(e). Both of them were then put into a small glass tube (inner diameter of 5 mm and total length of 20 mm) with the electrolyte consisting of 0.5M LiI, 0.05M I_2, and 0.5M 4-tert-butylpyridine in acetonitrile. Finally the tube was sealed with stuffing and epoxy, as depicted in Fig. 1(f). Figure 1(g) shows a fabricated 3D DSSC with lead wires.

The morphology and film thickness of the as-prepared samples was investigated using scanning electron microscopy (SEM, JEOL model JEM-6490). The dye adsorption was analyzed by ultraviolet-visible spectroscopy spectrophotometer (HITACHI, U-4100). The electrochemical activity of the electrode was measured by the cyclic voltammetry (CV) in a nitrogen saturated solution using a three-electrode cell in a PARSTAT 2273 potentiostat controlled by POWERSUITE software (Princeton Applied Research). Pt sheet and a saturated calomel electrode were used as the counter electrode and reference electrode, respectively. All potentials in this report are quoted versus Hg/Hg_2Cl_2. Electrochemical impedance spectroscopy (EIS) of the DSSC was also investigated
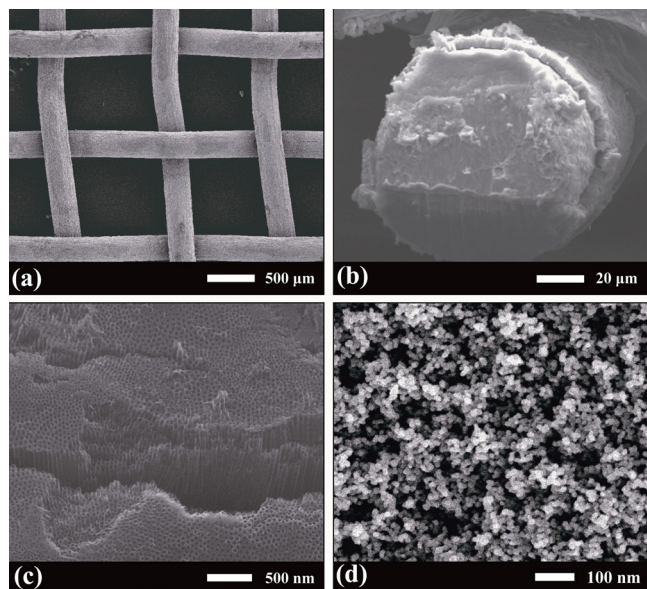
FIG. 2. (Color online) The morphology information of the electrodes: (a) The SEM image of the Ti mesh substrate (60-mesh). (b) Cross-sectional view SEM image of one anodized Ti wire from the Ti mesh. (c) Top view SEM image of the anodized Ti wire. (d) The top-view SEM image of the platinized Ti mesh.

FIG. 3. (Color online) Dependence of the amount of chemisorbed dye on the thickness of TiO$_2$ nanotube film based on three types of photoanodes (60-mesh, 90-mesh, and 120-mesh).

with the PARSTAT 2273 electrochemical analyzer. The applied bias voltage and ac amplitude were set at open-circuit voltage of the DSSCs and 10 mV between the two electrodes. The frequency range was 10^{-2}–10^5 Hz. A solar simulator (Newport-Oriel, 91192) served as a light source and the light intensity was adjusted with a reference Si cell for approximating 1 sun light intensity of 100 mW cm^{-2}. The I-V curves were measured with a Keithley 2400 source meter.

III. RESULTS AND DISCUSSIONS

Figure 2(a) is the SEM image of the Ti mesh substrate (60-mesh). The diameter of one Ti wire is about 100 μm which is one third of the side length of the opening. The electrolyte can diffuse through the openings to exchange electrons with electrodes. Figure 2(b) shows the cross sectional SEM image of one anodized Ti wire in the Ti mesh. It is apparent that after anodization a self-organized TiO$_2$ nanotube layer was *in situ* synthesized in perpendicular to the wire's surface with average length of 8.6 μm. As shown in Fig. 2(c), the nanotubes were packed in approximately cylindrical symmetry with an average inner diameter and wall thickness of 63 nm and 20 nm, respectively. Figure 2(d) is the top-view SEM image of the platinized Ti mesh. The Pt particles were distributed onto the Ti surface with the diameter range of 20–25 nm which implies that the Pt particles could provide sufficient surface area to exchange electrons with the electrolyte.

For the photoanodes of the DSSCs, the amount of dye adsorption is a key factor to enhance the light harvesting efficiency.[16] In order to determine the quantity of chemisorbed dye in the TiO$_2$ nanotube film, dye molecules were desorbed from a nominally identical batch of photoanodes in a mixed solution of 0.1M NaOH and ethanol (volume ratio:
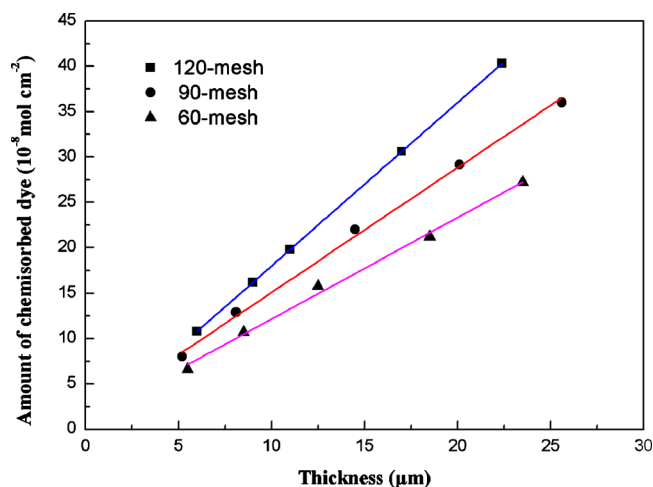
1:1). Figure 3 shows dependence of the amount of chemisorbed dye on the thickness of TiO$_2$ nanotube film based on three types of photoanodes. The amount of dye adsorption is proportional to the thickness of the TiO$_2$ nanotube film. Besides, for the same thickness TiO$_2$ nanotube film, the dye loading of the photoanode based on 120-mesh is the highest, followed by the one based on 90-mesh and then the one based on 60-mesh. This is probably due to the fact that, with the increase in the mesh number, the surface area of the Ti mesh substrate also increases, which means there will be larger surface area exposed for producing the TiO$_2$ nanotubes. As the amount of adsorbed dye strongly depends on the surface area of the TiO$_2$ nanotube film, the dye loading is enhanced.

The counter electrode of the DSSCs serves to transfer electrons from the external circuit to the electrolyte.[17] The role of Pt on the counter electrode is to catalyze the electrochemical reduction in the redox couple. An important parameter of the platinum-based counter electrode is the active surface area (A_s) of Pt because only the Pt atoms on the outside surface can contribute to the catalytic activity. As described in most electrochemical studies,[18,19] we measured the A_s of the three types of counter electrodes by using the hydrogen-desorption peaks on the CV curves in 0.5M H$_2$SO$_4$ aqueous solution. For comparison, all the counter electrodes were cut into 0.5 cm $\times$ 2 cm pieces with a Ti mesh (60-mesh) in the same size as the reference sample. Figure 4(a) shows the CV curves of the as-prepared counter electrodes and the reference sample. It is obvious that the Ti mesh showed no H adsorption–desorption features, which is in good agreement with the property of Ti substrates.[20] Consequently, the electro-oxidation peak in the CV curves of the platinized Ti mesh should be resulted from the existence of Pt. The A_s of the counter electrodes can be obtained according to the following equation:[21]

$$A_s = (Q_H/Q_e)A_{Pt}, \tag{1}$$

where Q_H represents the charges related to oxidization of monolayer hydrogen on the Pt surface, equaling to the cali-
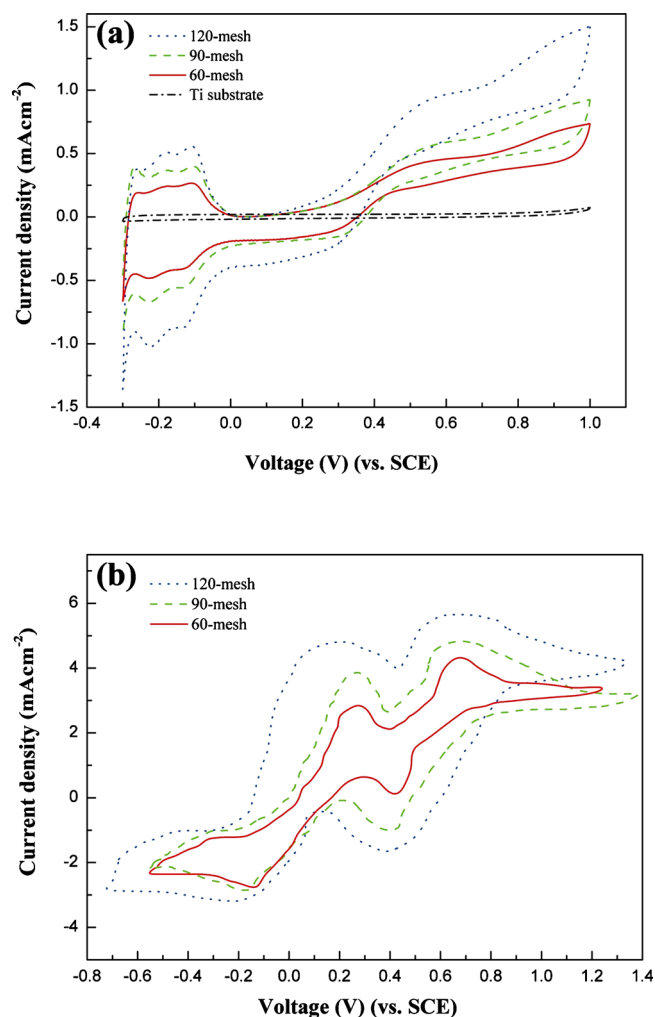
FIG. 4. (Color online) Cyclic voltammograms of three types of counter electrodes (60-mesh, 90-mesh, and 120-mesh) in (a) $0.5M$ H_2SO_4 aqueous solution; (b) the electrolyte solution, containing 5 mM LiI, 1 mM I_2, and $0.1M$ $LiClO_4$ as the supporting electrolyte in acetonitrile.

brated area of the hydrogen desorption peak on the CV curve; Q_e is the elementary charge ($Q_e = 1.602 \times 10^{-19}$ C); A_{Pt} is the averaged atomic area of surface Pt atoms and it is 7.69×10^{-20} m^2 according to the atomic density of Pt surface of about 1.3×10^{19} m^{-2}. This equation employs the well-established hydrogen-adsorption stoichiometry for the Pt surface (H:Pt=1:1).[22] Table I summarizes the electrochemical data obtained from the CV curves. Obviously, the A_s of the counter electrodes rises with the increment of the mesh number, which is in accordance with the trend of the dye loading on photoanodes discussed above. This result is

TABLE I. The electrochemical parameters of the counter electrodes obtained from the CV measurements.

Counter electrodes	Q_H (mC cm^{-2})	A_s (cm^2)
120-mesh	2.07	9.96
90-mesh	1.67	8.03
60-mesh	1.02	4.92
Ti mesh	0	0
Pt sheet	0.21	1.01

also attributed to the increased surface area of the Ti mesh substrate. In addition, for a flat smooth Pt sheet plate, Q_H is around 0.21 mC cm^{-2},[23,24] which means A_s is about 1.01 cm^2, only one-tenth of that of the 120-mesh counter electrode. It implies that the mesh structure based counter electrode could provide larger surface area for Pt atoms to disperse in than the one based on flat smooth sheet.

The increased A_s of the counter electrode with larger mesh number is further verified by the CV measurement in the electrolyte solution, containing 5 mM LiI, 1 mM I_2, and $0.1M$ $LiClO_4$ as the supporting electrolyte in acetonitrile. The CV curves of I^-/I_3^- redox couple on the three types of counter electrodes are shown in Fig. 4(b). It is observed that there are two anodic peaks in the anodic sweep and two cathodic peaks in the cathodic sweep, which were described in detail elsewhere.[25,26] The shapes of the curves are similar and the anodic and cathodic peak heights and areas increase along with the mesh number. We believe that the Ti mesh with larger mesh number could provide larger surface area for the platinum deposition, and hence the catalytic activity of Pt toward the reduction in I^-/I_3^- redox couple is enhanced.

EIS has been widely used[27,28] as a useful approach to investigate the influence of different resistance elements on the photoelectrochemical characteristics of the DSSCs. Generally, the impedance spectra of the DSSCs contains three semicircles,[29] which are attributed in terms of decreasing frequency to electrochemical reactions at the counter electrode/electrolyte interface (Z_1) in the high-frequency region, the electron transfer at the TiO$_2$/dye/electrolyte interface (Z_2) in the middle-frequency region, and the Nernst diffusion impedance of the redox species in the electrolyte (Z_3) in the low frequency region. The real parts of Z_1, Z_2, and Z_3 represent the resistance elements as R_1, R_2, and R_3, respectively. The resistive element R_h in the high-frequency region (around 100 kHz) corresponds to the sheet resistance of the substrate. To further explore the influence of the mesh number on the performance of the DSSCs, the electrodes based on different mesh number were assembled to fabricate the devices for EIS measurement. Figure 5 shows the variation in the EIS parameters of the DSSCs (under illumination of 100 mW cm^{-2} at open-circuit condition) by changing the mesh number of the electrodes. It could be seen when the mesh number of the photoanode was fixed to 60-mesh [Fig. 5(a)], with the increase in the mesh number on the counter electrode, the R_1 decreased from 57.6 to 15.5 Ω. Meanwhile, the R_2 and R_h remained nearly constant and R_3 increased from 40.1 to 60.5 Ω. Correspondingly, when the mesh number of the counter electrode was fixed to 60-mesh [Fig. 5(b)], with the increase in the mesh number on the photoanode, the R_2 decreased from 74.7 to 29.5 Ω; the R_1 and R_h kept constant and R_3 increased from 40.2 to 80.6 Ω. The decrease in R_1 in Fig. 5(a) is mainly caused by the increased active surface area (A_s) of Pt on the counter electrode. The reduction in R_2 in Fig. 5(b) attributes to the enhancement of the dye loading of the photoanode. For R_3, in both cases, with the increase in the mesh number, the diameter of the opening in the mesh is reduced, which causes the ions in the electrolyte more and more difficult to diffuse.
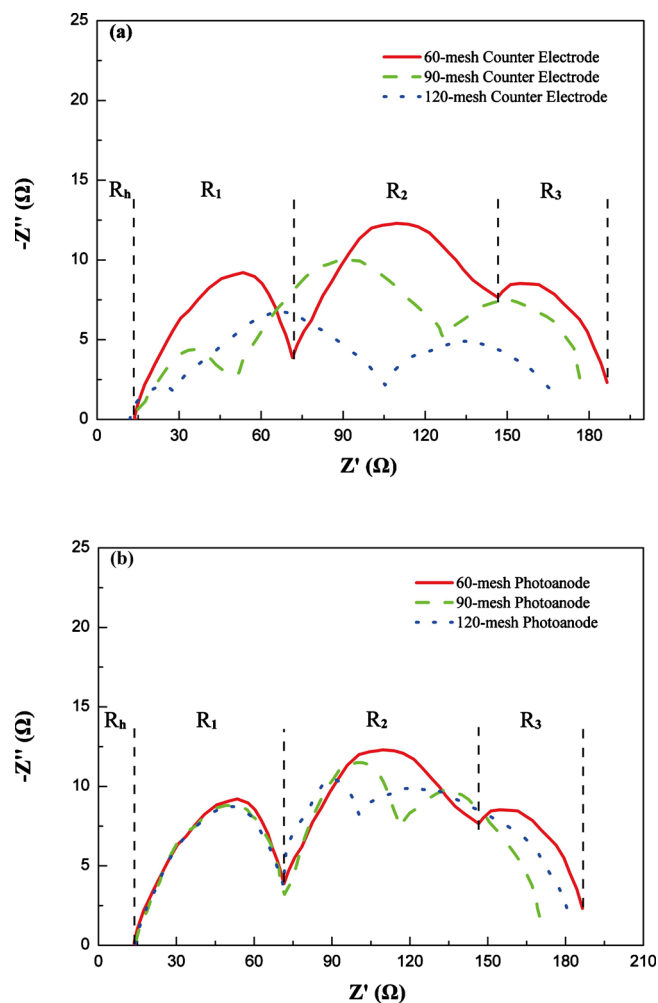
FIG. 5. (Color online) Electrochemical impedance spectra of the 3D DSSC (under 1 sun bias illumination at open-circuit condition) with different mesh number: (a) Photoanode: 60-mesh; counter electrode: 60-mesh, 90-mesh, and 120-mesh; (b) Photoanode: 60-mesh, 90-mesh, and 120-mesh; counter electrode: 60-mesh.

Hence, the R_3 will rise. Besides, as the substrates of this 3D DSSC are based on Ti metal, there is little change in the sheet resistance of the Ti mesh when the mesh number is varied. Consequently, the R_h has scarcely changed for the both cases. In general, the increase in the mesh number will lower R_1 and R_2 but enhance R_3 and have little impact on R_h.

In comparison with the other 3D DSSCs introduced in our previous work,[30,31] one of the merits of this new 3D DSSC is its superior light utilization efficiency. To confirm this point, the angle of the incident sunlight was changed from 0° to 180° and we measured the corresponding photovoltaic parameters of the device. As shown in Fig. 6, the short circuit current (I_{sc}) and open circuit voltage (V_{oc}) nearly remain unchanged with the variety of the incident angle, which demonstrates that the performance of this 3D DSSC is independent of the incident angle. This is because no matter which direction the constant light source irradiates from, the axial symmetrical structure of the 3D DSSC could capture the same quantity of the sunlight, as indicated in the inset of Fig. 6. Moreover, in the natural environment, cloudy skies may produce more scattered sunlight than the sunny skies.[32] Considering such sunlight may come from nearly all
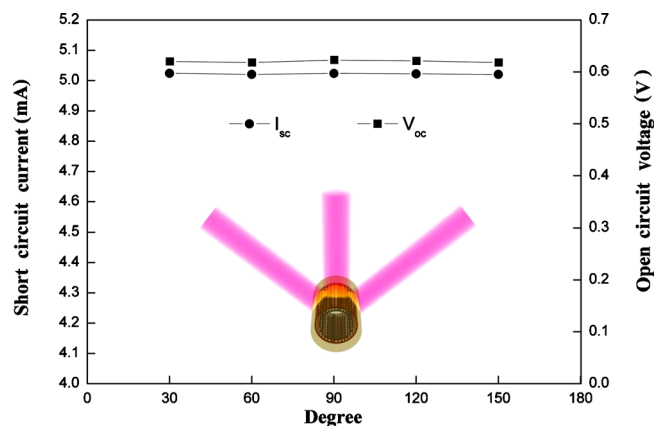

FIG. 6. (Color online) The photovoltaic parameters of the 3D DSSC illuminated in different angles of the incident sunlight. The inset shows the schematic diagram of the 3D DSSC under illumination in different angles.

skyward directions, this 3D DSSCs may work more efficiently than the flat types during cloudy days.

For the photovoltaic analysis, a series of the 3D DSSCs were fabricated by different combinations of photoanodes (60-mesh, 90-mesh, and 120-mesh) and counter electrodes (60-mesh, 90-mesh, and 120-mesh). We assume that the irradiated area of this 3D DSSC is the cross section of the cylinder which is a 5 mm×20 mm rectangle as shown in the inset of Fig. 7. Before the measurement, we first tried to optimize the thickness of the TiO$_2$ nanotube film on the photoanode because it is a key factor to influence the efficiency (η) of the DSSC. From Fig. 7 we could see the DSSC (60-mesh photoanode and 60-mesh counter electrode) with 14.5 μm showed the highest conversion efficiency (η) of about 3.2% with the short circuit current density (J_{sc}), open circuit voltage (V_{oc}), and FF of 6.30 mA cm^{-2}, 0.73 V, and 70.5%, respectively. As a result, we adopted 14.5 μm as the uniform film thickness by controlling the anodization time. Through several parallel experiments, we found the best combination was the 90-mesh photoanode with the 120-mesh counter electrode (η=5.5%), rather than the 120-mesh photoanode with the 120-mesh counter electrode (η=5.1%), as shown in Fig. 8. As discussed in the above, larger mesh
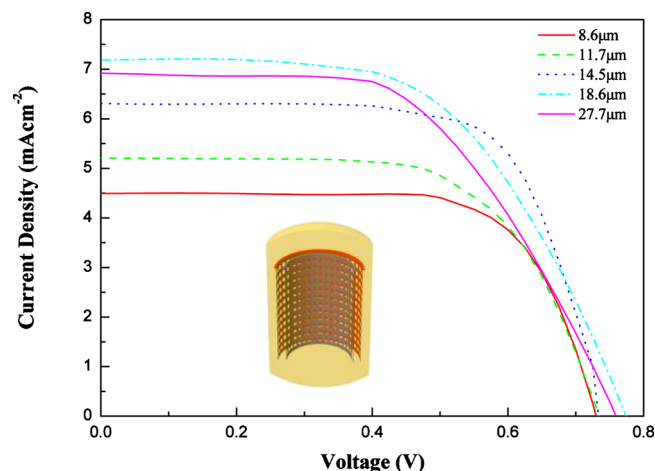

FIG. 7. (Color online) I-V performances of the 3D DSSCs with different lengths of nanotube layers. AM 1.5, 100 mW cm^{-2}. The inset shows the irradiated area of the 3D DSSC.
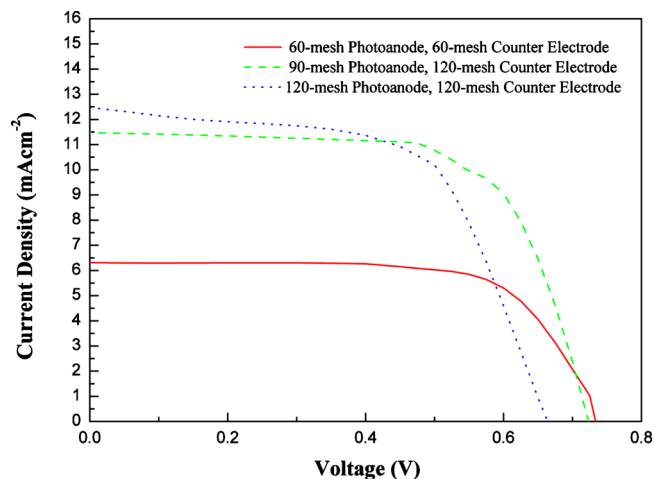
FIG. 8. (Color online) *I-V* performances of the 3D DSSCs based on 60-mesh photoanode with 60-mesh counter electrode, 90-mesh photoanode with 120-mesh counter electrode, and 120-mesh photoanode with 120-mesh counter electrode.

number is beneficial to the dye loading and active surface area (A_s) of Pt but it has a negative impact on the diffusion of the ions in the electrolyte. We believe this is the balanced result of these three factors.

Although this new 3D DSSC showed some superiority over traditional types, there are still some problems to be solved. For example, the sprayed SiO_2 layer on the counter electrode as the electrical insulator is sometimes easy to be broken, which causes the direct contact between the electrodes and lowers the efficiency of the cell. As a result, how to stabilize the electrical insulator layer is a key issue. Besides, the film thickness of the electrical insulator needs to be optimized since it determines the diffusion length of electrolyte. In addition to this, we are now investigating whether there are better ways of insulating the electrodes without blocking the transport of electrolyte, for example, to use a thin plastic mesh as the insulator. This work is currently in progress. We hope by sharing our ideas with other research groups, the photovoltaic performance of this 3D DSSC could be further optimized.

IV. CONCLUSIONS

In summary, we showed a new type of the 3D DSSC by utilizing the cylindrical Ti meshes as the substrates of electrodes. With the anodization method, a self-organized TiO_2 nanotube layer was *in situ* synthesized from the Ti mesh as the photoanode material. The morphologies of the electrodes were characterized by SEM. The influence of the mesh number was tested via the dye adsorption, CV curves, and EIS measurement. We found the dye loading on the photoanode as well as the active surface area of Pt on the counter electrode increased along with the mesh number but it was more difficult for the electrolyte to diffuse through the reduced-size openings in the mesh. In the photovoltaic analysis, the 3D DSSC based on 90-mesh photoanode and 120-mesh counter electrode exhibited the highest conversion efficiency of 5.5%. It was also demonstrated that the performance of this 3D DSSC is independent of the incident angle of the

solar radiation due to its axial symmetrical structure. Further work is to focus on optimizing the electrical insulator layer, and higher conversion efficiency is expected.

[1] B. G. Gribov and K. V. Zinov'ev, Inorg. Mater. **39**, 653 (2003).
[2] B. O'Regan and M. Grätzel, Nature (London) **353**, 737 (1991).
[3] M. Grätzel, Nature (London) **414**, 338 (2001).
[4] Y. Chiba, A. Isiam, Y. Watanabe, R. Komiya, N. Koide, and L. Han, Jpn. J. Appl. Phys., Part 2 **45**, L638 (2006).
[5] M. K. Nazeeruddin, F. De Angelis, S. Fantacci, A. Selloni, G. Viscardi, P. Liska, S. Ito, B. Takeru, and M. Grätzel, J. Am. Chem. Soc. **127**, 16835 (2005).
[6] A. Kay and M. Grätzel, Sol. Energy Mater. Sol. Cells **44**, 99 (1996).
[7] J. M. Kroon, N. J. Bakker, H. J. P. Smit, P. Liska, K. R. Thampi, P. Wang, S. M. Zakeeruddin, M. Grätzel, A. Hinsch, S. Hore, U. Würfel, R. Sastrawan, J. R. Durrant, E. Palomares, H. Pettersson, T. Gruszecki, J. Walter, K. Skupien, and G. E. Tulloch, Prog. Photovolt. Res. Appl. **15**, 1 (2007).
[8] K. Onoda, S. Ngamsinlapasathian, T. Fujieda, and S. Yoshikawa, Sol. Energy Mater. Sol. Cells **91**, 1176 (2007).
[9] X. M. Fang, T. L. Ma, M. Akiyama, G. Q. Guan, S. Tsunematsu, and E. Abe, Thin Solid Films **472**, 242 (2005).
[10] M. Paulose, K. Shankar, O. K. Varghese, K. G. Mor, B. Hardin, and C. A. Grimes, Nanotechnology **17**, 1446 (2006).
[11] X. Fan, F. Wang, Z. Chu, L. Chen, C. Zhang, and D. Zou, Appl. Phys. Lett. **90**, 073501 (2007).
[12] Y. Wang, Y. Liu, H. Yang, H. Wang, H. Shen, M. Li, and J. Yan, Curr. Appl. Phys. **10**, 119 (2010).
[13] Y. Wang, H. Yang, Y. Liu, H. Wang, H. Shen, J. Yan, and H. Xu, Prog. Photovoltaics **18**, 285 (2010).
[14] M. Adachi, I. Okada, S. Ngamsinlapasathian, Y. Murata, and S. Yoshikawa, Electrochem. **70**, 449 (2002).
[15] S. Ito, S. M. Zakeeruddin, P. Comte, P. Liska, D. Kuang, and M. Grätzel, Nat. Photonics **2**, 693 (2008).
[16] L. Yang, Y. Lin, J. Jia, X. Xiao, X. Li, and X. Zhou, Microporous Mesoporous Mater. **112**, 45 (2008).
[17] F. Cai, J. Liang, Z. Tao, J. Chen, and R. Xu, J. Power Sources **177**, 631 (2008).
[18] T. R. Ralph, G. A. Hards, J. E. Keating, S. A. Campbell, D. P. Wilkinson, M. Davis, J. S. Pierre, and M. C. Johnson, J. Electrochem. Soc. **144**, 3845 (1997).
[19] A. Pozio, M. De Francesco, A. Cemmi, F. Cardellini, and L. Giorgi, J. Power Sources **105**, 13 (2002).
[20] E. H. Yu, K. Scott, R. W. Reeve, L. Yang, and R. G. Allen, Electrochim. Acta **49**, 2443 (2004).
[21] D. Zhao and B. Xu, Angew. Chem. Int. Ed. **45**, 4955 (2006).
[22] J. Bett, K. Kinoshita, K. Routsis, and P. Stonehart, J. Catal. **29**, 160 (1973).
[23] M. Grden, A. Paruszewska, and A. Czerwinski, J. Electroanal. Chem. **502**, 91 (2001).
[24] L. dos Santos, F. Colmati, and E. R. Gonzalez, J. Power Sources **159**, 869 (2006).
[25] K. Imoto, K. Takahashi, T. Yamaguchi, T. Komura, J. Nakamura, and K. Murata, Sol. Energy Mater. Sol. Cells **79**, 459 (2003).
[26] Z. Huang, X. Liu, K. Li, D. Li, Y. Luo, H. Li, W. Song, L. Chen, and Q. Meng, Electrochem. Commun. **9**, 596 (2007).
[27] L. Han, N. Koide, Y. Chiba, A. Islam, R. Komiya, N. Fuke, A. Fukui, and R. Yamanaka, Appl. Phys. Lett. **86**, 213501 (2005).
[28] N. Koide, A. Islam, Y. chiba, and L. Han, J. Photochem. Photobiol., A **182**, 296 (2006).
[29] K. Lee, C. Hu, H. Chen, and K. Ho, Sol. Energy Mater. Sol. Cells **92**, 1628 (2008).
[30] Y. Liu, H. Wang, H. Shen, and W. Chen, Appl. Energy **87**, 436 (2010).
[31] H. Wang, Y. Liu, M. Li, H. Huang, H. Zhong, and H. Shen, Appl. Phys. A: Mater. Sci. Process. **97**, 25 (2009).
[32] I. Al-Turki and M. Schiler, Sol. Energy **59**, 241 (1997).